Electronic Supplementary Material (ESI) for Environmental Science: Advances.

Supplementary Information for:

Characterizing the hygroscopicity and volatility of single levitated aerosol droplet via optical tweezer-Raman spectroscopy

Yu-Kai Tong,[†] Teng Fang,[†] Zhijun Wu,[‡] Min Hu,[*,‡] and Anpei Ye[*,†]

†*Key Laboratory for the Physics and Chemistry of Nanodevices, School of Electronics, Peking University, Beijing 100871, China*

‡*State Key Joint Laboratory of Environmental Simulation and Pollution Control, College of Environmental Sciences and Engineering, Peking University, Beijing 100871, China*

E-mail: yap@pku.edu.cn; minhu@pku.edu.cn

S.1 Aerosol Trapping Chamber

Figure S1 Aerosol trapping chamber - (a) Overview, 1-Top cover with coverslip, 2-Chamber exterior, 3-Exhaust port, 4-Bottom baffle, 5&6-Fixing bolts and nuts, 7-Inlets for aerosols, nitrogen, and other possible substances; (b) Profile, 8-Bottom coverslip, 9-Top coverslip, 10-Inner cylinder baffle, 11-Rubber O-rings, 12&13-Fixing bolts and nuts. The path of incoming aerosol droplets and mixture of dry and wet nitrogen is expressed with red arrowed lines.

(a)

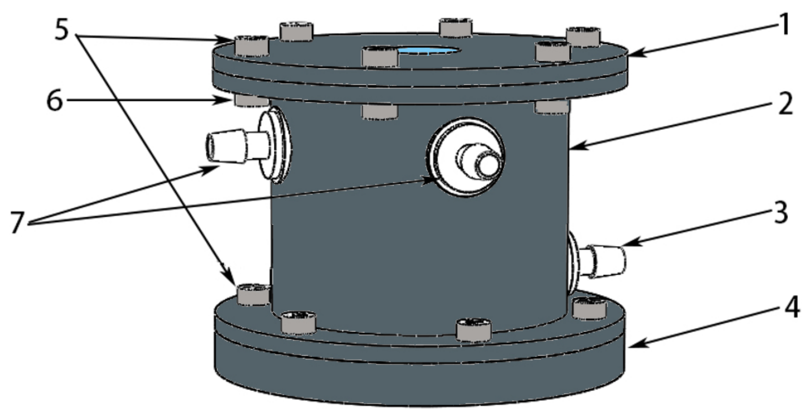

(b)

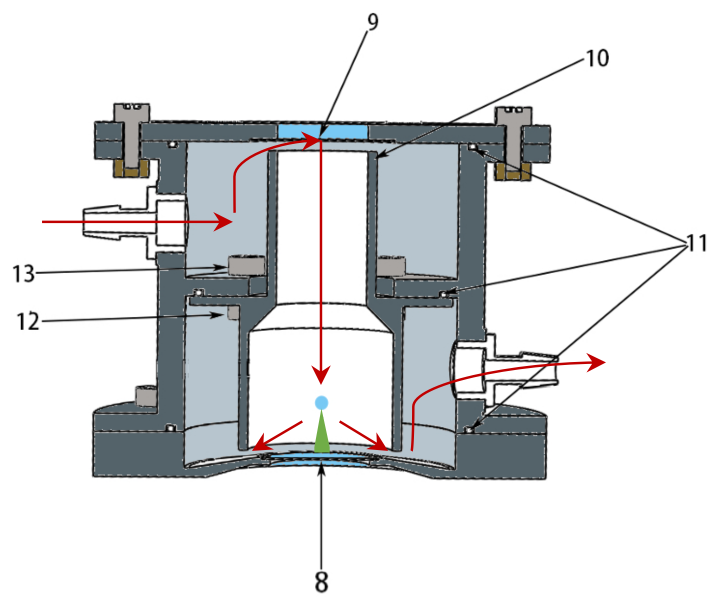

S.2 Performance of RH Controlling

Figure S2 RH Controlling - blue, the readouts of the RH probe when it was placed before the aerosol trapping chamber; red, the readouts of the RH probe when it was placed after the chamber. It can be seen that in both conditions the stability of the controlling was strikingly excellent when RH arrived at a pre-set value. The readouts plateaued to a constant value with a deviation below 0.1. Besides, when arriving at a same pre-set value, the readouts in both conditions were substantially identical whose discrepancy was below 1. However, when the RH was regulated, the response of the probe readouts before the chamber was faster than that after the chamber. The responding rate of the front position was around 2.89 %/min while that of the back position was around 1.84 %/mim. It could be in large part attributed to that the mixing dry/humidified nitrogen was buffered by the chamber and then decreased the regulating rate of the back position. Taken together, the position of the RH probe has a mild influence on the regulating performance of RH but no pronounced impacts on RH monitoring.

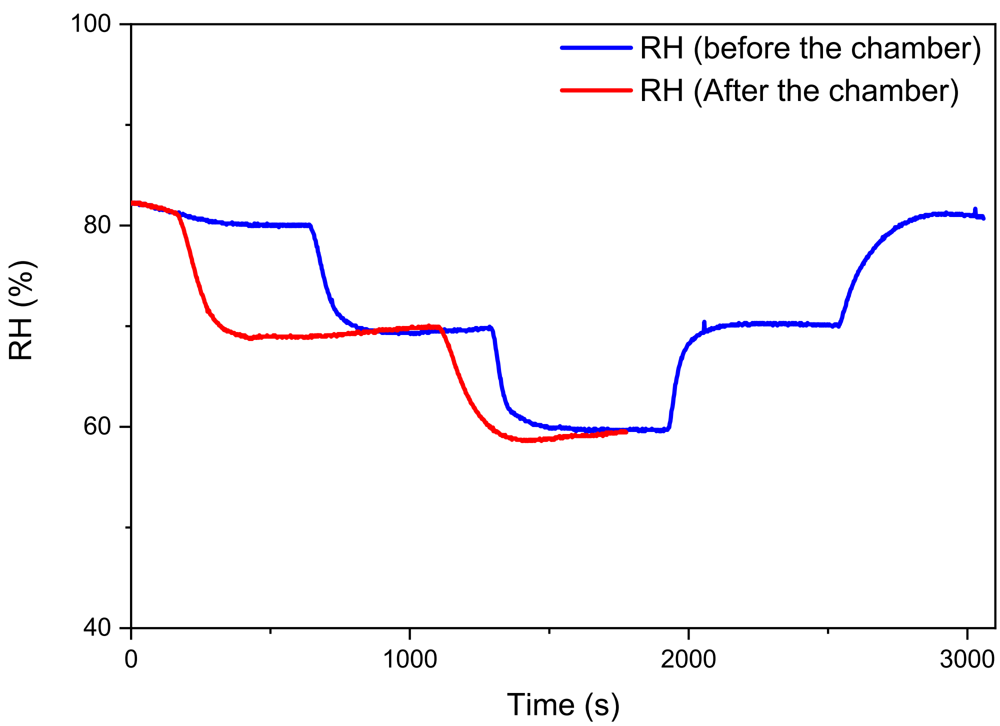

S.3 RI of CA droplet

Figure S3 Measured RI of CA Droplet - The RH remains constant at 50%. There are no obvious time-variations of RI during the volatile process of the CA microdroplet which indicates that the molarity of CA basically stays unchanged after reaching an equilibrium with ambient moisture. The c_0 in Eq. 3 in the main text is calculated according to the measured initial RI and the relationship of RI to molarity reported in CRC Handbook of Chemistry and Physics (J. Rumble, CRC Press, New York, 2021).

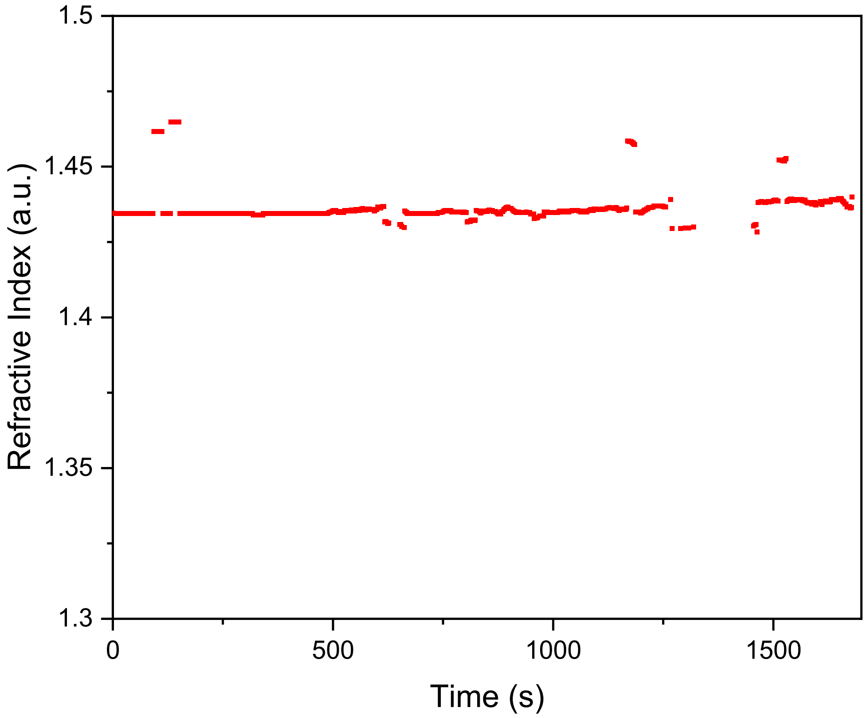

S.4 Discussions on the Influences of Laser Heating

Influences on diffusion coefficient

The heating from the laser beam may accelerate the transfer of water and lead the measured diffusion coefficients higher than the true values. For the shrinking process recorded in Fig. 4 (a2) in the main text, the temporal radius variation can be simplified as linear as follow,

$$r = r_0 - kt \tag{1}$$

where r is the real-time radius of the droplet, r_0 is the initial radius, t is the time, and k is the slope of the radius variation. If there is no laser heating, the radius can be modified as

$$r = r_0 - \lambda kt \tag{2}$$

where λ ($0 < \lambda <1$) is the modifying factor.

According to Eq. 2 in the main text, the size decreasing process under two conditions can be specified as

$$\begin{aligned} \frac{r_0^3 - (r_0 - kt)^3}{r_0^3 - (r_0 - k\tau)^3} &= \frac{6}{r_0}\sqrt{\frac{D_A t}{\pi}} \\ \frac{r_0^3 - (r_0 - \lambda kt)^3}{r_0^3 - (r_0 - \lambda k\tau)^3} &= \frac{6}{r_0}\sqrt{\frac{D_B t}{\pi}} \end{aligned} \tag{3}$$

where τ is the consumed time when the droplet achieves a balance with the ambient moisture after a sufficient mass transfer, D_A and D_B are the apparent water diffusion coefficients under the condition with/without laser heating respectively. Then, the variation of the diffusion coefficient can be derived as

$$\sqrt{\frac{D_B}{D_A}} = \frac{1 - (1 - \frac{\lambda kt}{r_0})^3}{1 - (1 - \frac{kt}{r_0})^3} \cdot \frac{1 - (1 - \frac{k\tau}{r_0})^3}{1 - (1 - \frac{\lambda k\tau}{r_0})^3} \tag{4}$$

Denoting kt/r_0 by ξ (for a size decreasing process, $0 \leq \xi < 1$), we can derived that

$$\frac{1-(1-\frac{\lambda kt}{r_0})^3}{1-(1-\frac{kt}{r_0})^3} = \frac{1-(1-\lambda\xi)^3}{1-(1-\xi)^3} = \mathcal{F}(\xi) \tag{5}$$

For the result shown in Fig. 4 (a2), it can be found that $k\tau/r_0 = 200/5900 = 0.034$. Assuming that the variation of droplet radius under the same RH step in Fig. 4 (a2) is only several tens of nanometers in the absence of laser heating, the λ can be plausibly taken as 0.1. Then $\mathcal{F}(\xi) < \mathcal{F}(\xi \to 1) = 0.27$ and $\mathcal{F}(\xi) > \mathcal{F}(\xi \to 0) = 0.1$, so $(D_B/D_A) < (0.27 \times 9.7)^2 = 6.8$ and $(D_B/D_A) > (0.1 \times 9.7)^2 = 0.94$. It indicates that the deviation caused by the laser heating effect is lower than one order of magnitude (-0.03 $<$log $(D_B/D_A)<$ 0.8). Considering the relatively wide discrepancies of the literature values listed in Tab. 1 in the main text, the reported values herein are still meaningful.

Influences on volatility

As done above, according to Eq. 3 in the main text, the volatile flux under two conditions can be specified as

$$\begin{aligned} [r_0^3 - (r_0 - kt)^3]c_0 &= 3F_A(r_0 - kt)^2 t \\ [r_0^3 - (r_0 - \lambda kt)^3]c_0 &= 3F_B(r_0 - \lambda kt)^2 t \end{aligned} \tag{6}$$

where F_A and F_B are the volatile fluxes under the condition with/without laser heating respectively. Then, the variation of the volatile flux can be derived as

$$\frac{F_B}{F_A} = \frac{r_0^3 - (r_0 - \lambda kt)^3}{r_0^3 - (r_0 - kt)^3} \cdot \frac{(r_0 - kt)^2}{(r_0 - \lambda kt)^2} \tag{7}$$

Denoting kt/r_0 by ξ, Equation 7 can be rewritten as

$$\frac{F_B}{F_A} = \frac{1-(1-\lambda\xi)^3}{1-(1-\xi)^3} \cdot \frac{(1-\xi)^2}{(1-\lambda\xi)^2} = \mathcal{F}(\xi) \cdot \mathcal{G}(\xi) \tag{8}$$

For the result shown in Fig. 5 (a), it can be found that $0 \leq \xi \leq 2/7$. Taking λ as 0.1, we can derive that $0.1 = \mathcal{F}(\xi \to 0) < \mathcal{F}(\xi) < \mathcal{F}(\xi \to 2/7) = 0.131$ and $0.54 = \mathcal{G}(\xi \to 2/7) < \mathcal{G}(\xi) < \mathcal{G}(\xi \to 0) = 1$. Thus, there will be $0.054 < (F_B/F_A) < 0.131$; the deviation caused by the laser heating might be higher than one order of magnitude ($-1.26 < \log(F_B/F_A) < -0.88$). The calculated error coefficient (i.e. the mean of the upper and lower bound of F_B/F_A) is presented in the main text.